Science of the Total Environment 806 (2022) 150365

Contents lists available at ScienceDirect

Science of the Total Environment

journal homepage: www.elsevier.com/locate/scitotenv

Quantitative proteomics reveals tissue-specific toxic mechanisms for acute hydrogen sulfide-induced injury of diverse organs in pig

Zhen Liu [a,b,1], Liang Chen [a,1], Xin Gao [c,1], Ruixia Zou [d], Qingshi Meng [a], Qin Fu [e], Yanjiao Xie [a], Qixiang Miao [a], Lei Chen [a], Xiangfang Tang [a,*], Sheng Zhang [e], Hongfu Zhang [a,*], Martine Schroyen [b]

[a] State Key Laboratory of Animal Nutrition, Institute of Animal Sciences, Chinese Academy of Agricultural Sciences, Beijing 100193, China
[b] Precision Livestock and Nutrition Unit, Gembloux Agro-Bio Tech, TERRA Teaching and Research Centre, University of Liège, Passage des Déportés 2, Gembloux 5030, Belgium
[c] State Key Laboratory of Veterinary Etiological Biology, Lanzhou Veterinary Research Institute, Chinese Academy of Agricultural Sciences, Lanzhou 730046, China
[d] Graduate School, Chinese Academy of Agricultural Sciences, Beijing 100081, China
[e] Proteomics and Metabolomics Facility, Institute of Biotechnology, Cornell University, Ithaca, NY 14853, USA

HIGHLIGHTS

- Acute H_2S exposure affected porcine lung, trachea and liver tissues via different mechanisms.
- The toxic mechanisms of acute H_2S exposure in the lung and trachea are relatively similar.
- Complement and coagulation cascades, antigen presentation and hyaluronan metabolism were implicated in lung.
- Complement and coagulation cascades, oxidative stress, cell apoptosis and hyaluronan metabolism were implicated in trachea.
- Acute H_2S exposure induced liver dysfunction via affecting protein synthesis and lipid metabolism.

GRAPHICAL ABSTRACT

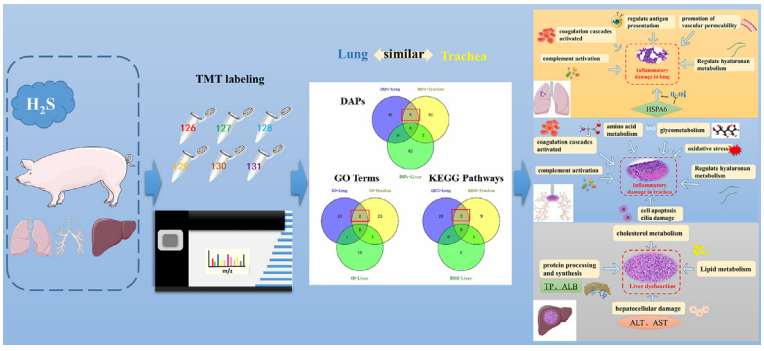

ARTICLE INFO

Article history:
Received 25 July 2021
Received in revised form 9 September 2021
Accepted 12 September 2021
Available online 16 September 2021

Editor: Henner Hollert

Keywords:
H_2S
Acute exposure
TMT-based proteomics
Multi-organ injury
Porcine
Inflammatory injury

ABSTRACT

Hydrogen sulfide (H_2S) is a highly toxic gas in many environmental and occupational places. It can induce multiple organ injuries particularly in lung, trachea and liver, but the relevant mechanisms remain poorly understood. In this study, we used a TMT-based discovery proteomics to identify key proteins and correlated molecular pathways involved in the pathogenesis of acute H_2S-induced toxicity in porcine lung, trachea and liver tissues. Pigs were subjected to acute inhalation exposure of up to 250 ppm of H_2S for 5 h for the first time. Changes in hematology and biochemical indexes, serum inflammatory cytokines and histopathology demonstrated that acute H_2S exposure induced organs inflammatory injury and dysfunction in the porcine lung, trachea and liver. The proteomic data showed 51, 99 and 84 proteins that were significantly altered in lung, trachea and liver, respectively. Gene ontology (GO) annotation, KEGG pathway and protein-protein interaction (PPI) network analysis revealed that acute H_2S exposure affected the three organs via different mechanisms that were relatively similar between lung and trachea. Further analysis showed that acute H_2S exposure caused inflammatory damages in the porcine lung and trachea through activating complement and coagulation cascades, and regulating the hyaluronan metabolic process. Whereas antigen presentation was found in the lung but oxidative stress and cell apoptosis was observed exclusively in the trachea. In the liver, an induced dysfunction

* Corresponding authors.
E-mail addresses: tangxiangfang@caas.cn (X. Tang), zhanghongfu@caas.cn (H. Zhang).
[1] These authors contributed equally to this work.

https://doi.org/10.1016/j.scitotenv.2021.150365

was associated with protein processing in the endoplasmic reticulum and lipid metabolism. Further validation of some H_2S responsive proteins using western blotting indicated that our proteomics data were highly reliable. Collectively, these findings provide insight into toxic molecular mechanisms that could potentially be targeted for therapeutic intervention for acute H_2S intoxication.

1. Introduction

Hydrogen sulfide (H_2S), as a gaseous compound in the atmosphere, is an important air pollutant threatening human health (Ausma and De Kok, 2019; Lewis and Copley, 2015). It can be produced in a variety of human activity places including oil and gas industry, intensive animal farming industry, in paper mills and waste water purification facilities, and so on (Saiyed, 2006). It is the second leading cause of acute fatal gas exposure in the working environment, being below the carbon monoxide (Guidotti, 2010). Besides exposures under environmental and industrial settings, intentional H_2S poisoning for suicide has recently increased in Western and Asian societies (Morii et al., 2010; Reedy et al., 2011). There are concerns of potential nefarious use of H_2S as a chemical weapon by terrorists, which will bring a major risk to victims and first responders (Ng et al., 2019). Short-term effects of acute exposure to H_2S concentrations greater than 100 ppm include olfactory paralysis, pulmonary edema, ataxia, dyspnea, unconsciousness ("knockdown"), seizures, cardiac arrhythmias, and ultimately death (Kim et al., 2018; Reiffenstein et al., 1992).

As a broad-spectrum toxicant, the exposure of H_2S is known to cause toxic effects on many organ systems including the respiratory, nervous, cardiovascular and digestive systems in human and animals (Anantharam et al., 2017; Chen et al., 2019; Schroeter et al., 2006; Yin et al., 2020). In mice, inflammatory pathological damages were observed in the lung after 1 h after injection of exogenous H_2S (NaHS, 14 pmol/kg) (Li et al., 2005). In chicken, 20 ppm H_2S exposure for three weeks caused inflammatory damages in the trachea by inducing oxidative stress (Chen et al., 2019) or induced apoptosis and necroptosis in the trachea through lncRNA3037/miR-15a/BCL2-A20 signaling (Li et al., 2020). It has been reported that H_2S exposure induces immune dysregulation and cell death in the broiler thymus by activating JNK/MST1/FOXO1 pathway (Chi et al., 2021) and exacerbates LPS-induced hepatocyte autophagy via the PI3K/AKT/TOR pathway in the chicken (Guo et al., 2021). In human, low concentration H_2S exposure resulted in headaches, nausea, and respiratory problems (Guidotti, 2015). Data from humans undergoing mass exposure to acute H_2S suggested that about 75% of the victims suffered clinical symptoms such as breathing difficulties and pulmonary edema, while 5% cases after the exposure were fatal (Burnett et al., 1977; Malone Rubright et al., 2017; Snyder et al., 1995). Up to now, there is no suitable antidote available for treatment of H_2S-induced toxicity while study on developing the effective antidote for H_2S poisoning is limited (Hendry-Hofer et al., 2020; Kim et al., 2018). Given the H_2S's threat to public health, and its mechanisms of resulting pathologies are unclear, more mechanistic study on the toxicological effects of acute exposure of H_2S is necessary.

Because of their similar physiological activity, anatomical structure and metabolism, pigs are widely used in nutritional and medical research for human (Bassols et al., 2014; Roura et al., 2016). Pigs therefore become a good model for studying the toxicological effects of acute H_2S exposure, and such research may lead to develop therapeutic treatments for H_2S poisoning. In this study, we established an H_2S poisoning model via the acute exposure to 250 ppm H_2S on pigs for the first time. Compared with the animal model performed with anesthetized animals in a H_2S inhalation exposure or sodium hydrosulfide injection model, it is a better mimic for existing H_2S poisoning cases in humans (Jiang et al., 2016; Sonobe et al., 2015). This study aimed to use this pig model to investigate proteomic changes in major respiratory and metabolic organs (lung, trachea and liver) following acute hydrogen sulfide exposure in order to shed new light on toxic molecular mechanisms that could be potentially targeted for therapeutic intervention or provide valuable information for the development of novel antidotes or therapies for acute H_2S intoxication.

2. Methods

2.1. Materials and methods

2.1.1. Animal experiment and sample collection

All procedures of the animal experiments in this study were approved by the Experimental Animal Welfare and Ethical Committee of Institutes of Animal Sciences, Chinese Academy of Agricultural Sciences (IAS2018-25). Twelve pigs (*sus scrofa*) (weighing 12.09 ± 0.33 kg, 6 male and 6 female) were purchased from a local Large White pig breeding farm (Beijing, China) and raised in environmentally controlled chambers. Pigs were randomly allocated into two groups labeled as H_2S group and Control group, respectively. Six pigs in the Control group were raised in a separate chamber without H_2S while 6 pigs in the H_2S group were exposed to 250 ppm H_2S for 5 h based on previously published literature indicating concentrations during 200–300 ppm can induce significant effects on the respiratory system after extended exposure (>1 h) in human (Guidotti, 2010, 2015; Hughes et al., 2009). During the experimental period, pigs were given ad libitum access to feed and water. The ambient parameters of each chamber including temperature, light time, relative humidity and any other environmental parameters were kept consistent. At the end of the animal experiment, blood was collected from the jugular vein using a sterilized syringe. A total of 6 ml blood was collected into tubes coated with EDTA-Na2 for blood routine, and into anticoagulant-free tubes for biochemistry assays and ELISA analysis. The blood tubes without anticoagulant were incubated at 37 °C for 30 min, followed by centrifugation at 3000 rpm for 15 min to collect serum, and stored at −20 °C until biochemical analysis and ELISA assays. Pigs were euthanized for the collection of lung, trachea and liver samples by electric stunning at the end of this experiment. An aliquot was fixed in 4% paraformaldehyde, while the remainder was snap frozen in liquid nitrogen and then stored at −80 °C until further analysis.

2.1.2. Measurement of blood routine indices and serum biochemical indexes

The blood routine analysis was performed using an automatic hematology analyzer (TEK-II mini, Tecom Science, China). The parameters included white blood cell counts (WBC, 10^9/l), granulocyte counts (GRA, 10^9/l) and percentage (GRA%, %), red blood cell counts (RBC, 10^{12}/l), hemoglobin concentration (HGB, g/l), hematocrit (HCT, L/l) and blood platelet counts (PLT, 10^9/l). Serum biochemical parameters including total protein (TP, g/l), albumin (ALB, g/l), alanine aminotransferase (ALT, U/l), aspartate aminotransferase (AST, U/l), immunoglobulin A (IgA, g/l), immunoglobulin M (IgM, g/l) and immunoglobulin G (IgG, g/l) were measured by an automatic biochemistry analyzer (DxC 600, Beckman Coulter, USA).

2.1.3. Enzyme-linked immunosorbent assay (ELISA) analysis of serum cytokines

The concentrations of cytokines related to inflammatory response, including TNF-α, IL-1β, IL-6, and IL-10 in the serum were tested using ELISA kits according to the instructions of the manufacturer (Sinogene Biotech Co., Ltd., Beijing, China).

2.1.4. Morphological examination

Lung, trachea and liver tissues were fixed in 4% paraformaldehyde for at least 24 h. Then the tissues were dehydrated in ethanol, immersed in paraffin, cut into slices, and stained with hematoxylin and eosin (HE) respectively. Histological changes of these tissues were scanned with an automatic digital slide scanner (Pannoramic MIDI, 3D HISTECH, Hungary).

2.1.5. Proteomics analysis

2.1.5.1. Protein extraction. Approximately 100 mg of frozen tissues (lung, trachea and liver) for each of the 6 pigs (randomly chose from the 12 pigs)were homogenized in 500 μl extraction buffer (100 mM Tris-HCl, 4% SDS, 20 mM NaCl, 50 mM DTT, pH 7.88) for 5 min. The lysates were boiled at 95 °C for 5 min, and centrifuged at 20,000 ×*g* for 15 min (25 °C), and the supernatants were transferred into a clean tube. BCA assay kit (Thermo Fisher, USA) was used to measure the protein concentration for each sample.

2.1.5.2. Protein digestion. Dithiothreitol (DTT) was added into 50 μg protein extracts of each of individual sample with a final concentration of 20 mM for reduction by incubation at 50 °C for 30 min. Followed by iodoacetamide (IAA) alkylation with a final concentration of 100 mM and incubation in darkness for 30 min. The alkylated proteins were precipitated in seven volumes of cold acetone and incubated at −20 °C overnight. Subsequently, the protein solutions were centrifuged at 20,000 ×*g* for 15 min at 4 °C. The supernatants were discarded, and the precipitated protein pellet was resuspended in 100 μl of 50 mM triethylammonium bicarbonate (TEAB). The samples were digested with trypsin (Promega, USA) at a ratio of 1:50 for 12 h (37 °C).

2.1.5.3. TMT labeling. The TMT-6 plex Label Reagent Kit (Thermo Scientific, USA) was equilibrated to room temperature immediately before use. The TMT 6-plex labels (126, 127, 128, 129, 130, 131) (dried powder) were reconstituted with 41 μl of anhydrous acetonitrile prior to labeling and added to each of the 100 μl tryptic digest samples and incubated for 1 h at room temperature. The labeling reactions were stopped by adding 8 μl of 5% hydroxylamine and incubating for 15 mins, and the TMT labeled peptides of each sample were pooled in equal proportion.

2.1.5.4. Reverse-phase high-performance liquid chromatography (RP-HPLC) fractionation. RP-HPLC was carried out using an Agilent 1290 LC System (Agilent, USA) by TechMate C18-ST (5 μm, 4.6 × 250 mm) to separate the tagged peptides. Mobile phase A consisted of 10 mM ammonium formate pH 10.0 in water and mobile phase B contained 10 mM ammonium formate pH 10.0 in acetonitrile. LC was carried out at a flow rate of 1 ml/min during a 36 min gradient from 5 to 60% of buffer B. Forty fractions were collected at 1 min intervals and pooled into ten fractions based on UV absorbance at 214 nm. Then, each fraction was dried and reconstituted for subsequent nanoLC-MS/MS analysis.

2.1.5.5. NanoLC-MS/MS analysis. Each fraction was reconstituted with 2% acetonitrile and 0.1% formic acid. A nano LC-MS/MS analysis was carried out using an Orbitrap Fusion Tribrid MS (Thermo Scientific, San Jose, CA) with a nanospray flex ion source coupled with a Dionex UltiMate 3000 RSLC nano system (Thermo, Sunnyvale, CA). Peptide samples (2 μl) were injected into the PepMap C18 columns (75 μm × 3 mm, 3 μm) at 6 μl/min for on-line enrichment and then separated on a PepMap C18 column (75 μm × 250 mm, 2 μm) with 0.1% formic acid as buffer A and 0.1% formic acid in 80% acetonitrile as buffer B at 300 nl/min. The peptides elution was performed under the following gradient program: 0–5 min, 5–12% B; 5–65 min, 12%–38% B; 65–72 min, 38–95% B; 72–80 min, 95% B; 80–81 min, 95–5% B; and 81–95 min, 5% B. The mass spectrometer was operated using electrospray ionization (2 kV) at 275 °C. The Orbitrap resolving power was set 120,000 (at *m/z* 200) for MS1, and 30,000 for MS/MS scans. The MS/MS spectra were acquired using a quadrupole isolation width of 1.2 m/z and HCD normalized collision energy (NCE) of 38. Dynamic exclusion was set for 30 s using monoisotopic precursor selection.

2.1.5.6. Data analysis. The *Sus scrofa* database (UP000008227) downloaded from Uniprot was used for database searches. The default search settings used for protein identification and quantitation in MaxQuant software (v 1.6.4) were: fixed modification of carbamidomethyl (C) and TMT6-plex on K and N-terminus, variable modification of oxidation (M) and deamidated (NQ), 10 ppm peptide mass tolerance and 10 mDa fragment mass tolerance, and two missed cleavages allowed. Maximum false discovery rates (FDRs) for peptide and protein identification were specified as 1%. The proteins with a fold change > 1.2 along with p-value < 0.05 were considered as differentially accumulated proteins (DAPs).

2.1.5.7. Western blotting analysis. Total protein was extracted using the RIPA Lysis Buffer (SinoGene, Beijing, China). Proteins were separated by electrophoresis on 12% SDS-PAGE gels and transferred to PVDF membranes in tris-glycine transfer buffer. Membranes were blocked with Fast Protein-free Block Buffer (SinoGene, Beijing, China) at room temperature for 5 mins, and then incubated with primary antibodies (Abcam, China) at 4 °C overnight. Specific reaction products were incubated with horseradish peroxidase (HRP)-conjugated secondary antibody (Abcam, China) at room temperature for 1 h. Finally, the signal was detected on a Universal Hood III (Bio-Rad, USA) using the ECL Substrate reagent (Engreen, Beijing, China). The protein levels in each sample were normalized by β-actin (Abclonal, China). Detailed antibody information is shown in Supplemental Table 1.

2.1.5.8. Bioinformatics analysis. Gene Ontology (GO) annotation and Kyoto Encyclopedia of Genes and Genomes (KEGG) pathway enrichment for the DAPs were analyzed by the KOBAS 3.0 database (http://kobas.cbi.pku.edu.cn/). GO terms and pathways with a corrected (Benjamini-Hochberg) p-value <0.05 were considered significantly enriched. The protein-protein interaction (PPI) network analysis of the DAPs was performed by the STRING 11.0 database (https://string-db.org/). Visualization of volcano plot analyses, hierarchical clusters and bioinformatic analyses in this study were performed using the OmicStudio (https://www.omicstudio.cn/tool), OmicShare (http://www.omicshare.com/tools) and RStudio (https://www.rstudio.com/).

2.1.6. Statistical analysis

Statistical analysis was performed by SPSS (version 23.0, IBM, USA) using the independent t-test. All data are presented as mean ± standard error. Differences were assumed to be statistically significant when p-value < 0.05.

3. Results

3.1. Acute H_2S exposure induced systemic immune response, hypoxia, and liver dysfunction in pig

We examined the hematological changes and specific serum biochemical indexes related to immune responses, and liver functions in blood and serum of pig (Fig. 1). The results showed that WBC, GRA, GRA%, RBC, HGB, HCT were significantly increased while PLT was significantly decreased in the porcine blood after an acute H_2S exposure (Fig. 1A–G). Serum biochemical indexes: TP and ALB were significantly decreased while AST, ALT, IgA and IgM were significantly increased in the porcine serum after an acute H_2S exposure (Fig. 1H–M), whereas the levels of IgG were similar in the two groups (Fig. 1N). Serum concentrations of proinflammatory factors, including TNF-α, IL-1β and IL-6 were consistently increased (Fig. 2A–C), and the concentration of

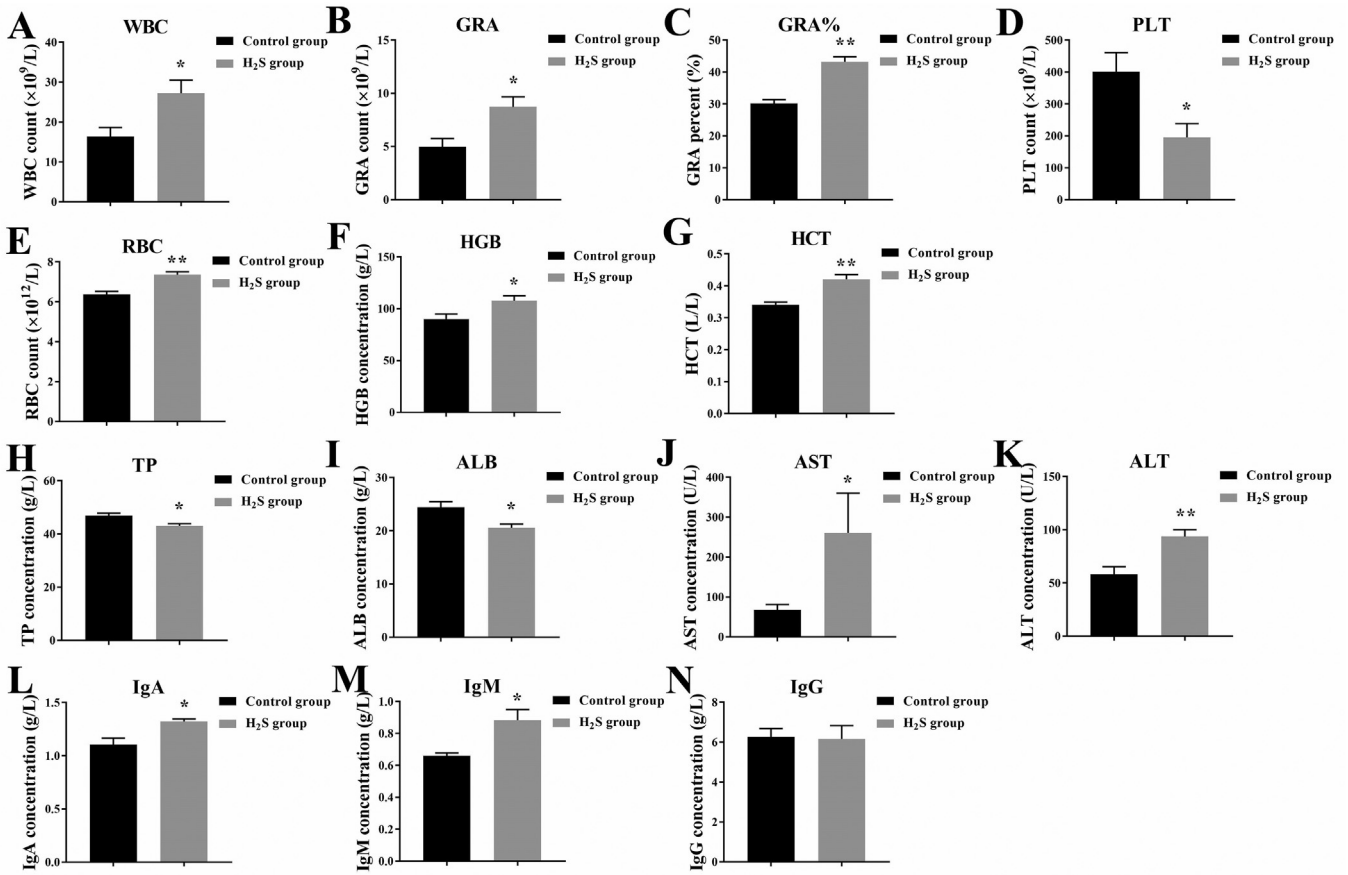

Fig. 1. Acute H_2S exposure induced systemic immune response and hypoxia, and dysfunction in liver of pig (Control group, $n = 6$; H_2S group, $n = 6$). (A-G) Key blood routine indices related to immune response and oxygen transport tested in blood of pig. (H—N) Serum biochemical indexes related to immune responses and liver functions tested in serum of pig. * indicates p-value < 0.05, ** indicates p-value < 0.01.

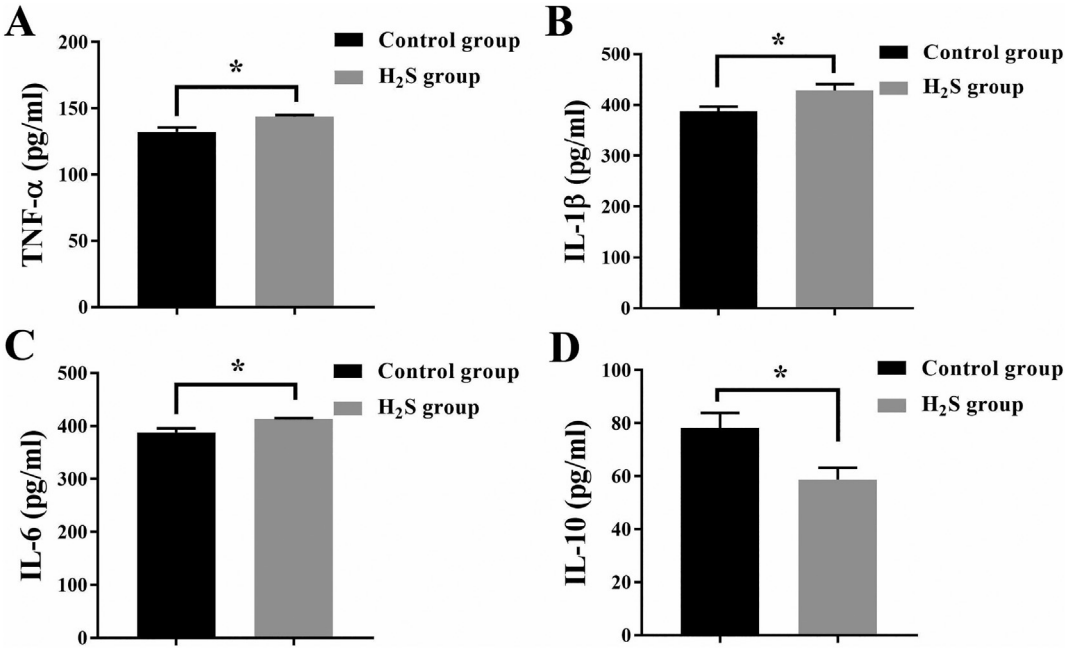

Fig. 2. Acute H_2S exposure induced systemic inflammatory response in pig (Control group, $n = 6$; H_2S group, $n = 6$). Key cytokines related to inflammatory response in serum of pig, including TNF-α (A), IL-1β (B), IL-6 (C) and IL-10 (D). * indicates p-value < 0.05.

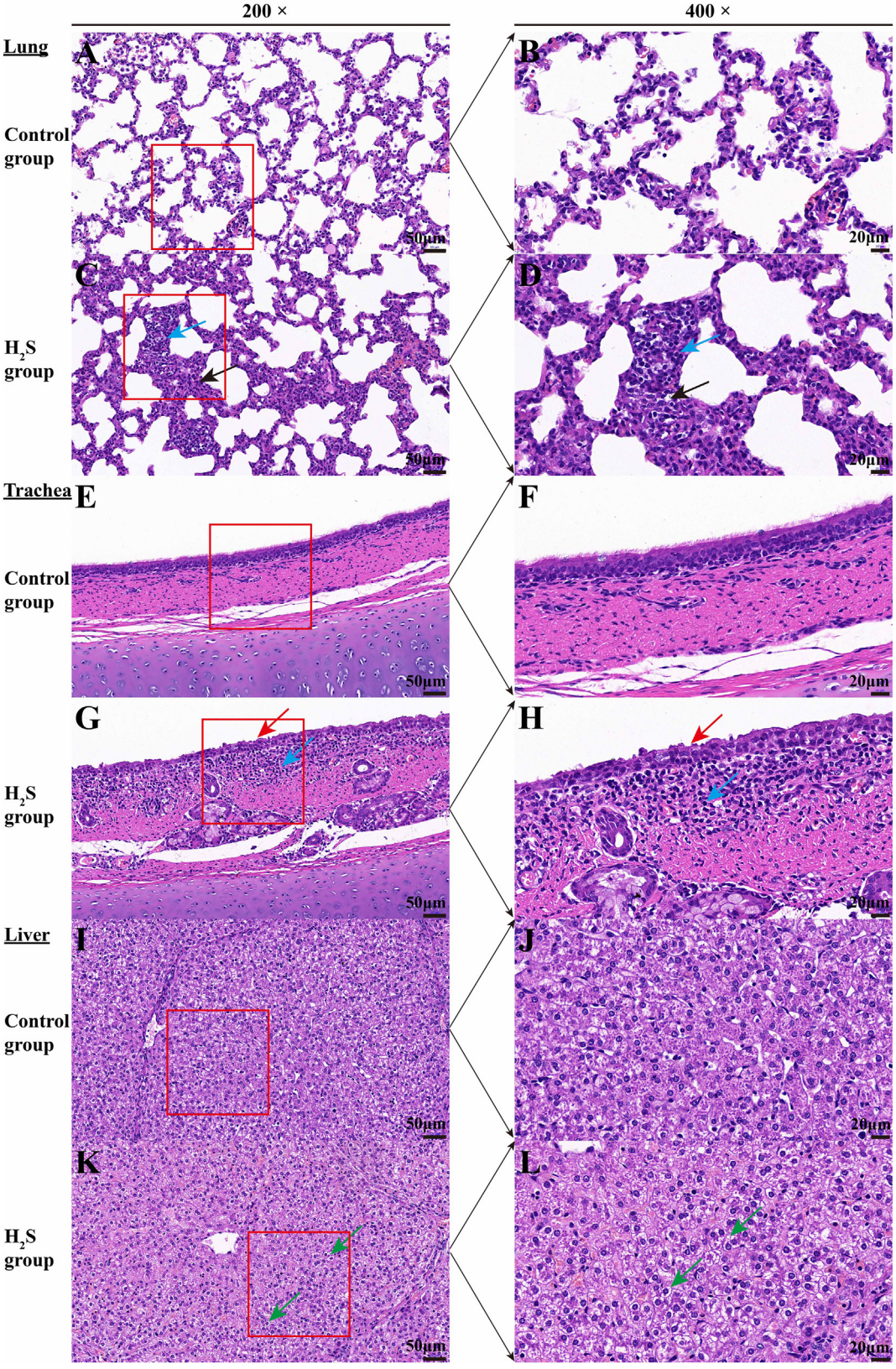

Fig. 3. Acute H_2S exposure induced inflammatory injury and histopathology changes in lung, trachea and liver of pig (Control group, $n = 6$; H_2S group, $n = 6$). Morphological examination of lung (panels A, B, C, D), trachea (panels E, F, G, H) and liver tissues (panels I, J, K, L) by H.E. staining in the Control group and the H_2S group. The left two pictures for each tissue (A, C, E, G, I, K) are in the 200×, the right two (B, D, F, H, J, L) are in the 400× magnification. The blue arrows indicate inflammatory cell infiltration, the black arrows indicate hyperplasia, the red arrows indicate disruption and desquamation and the green arrows indicate vacuolation. (For interpretation of the references to colour in this figure legend, the reader is referred to the web version of this article.)

anti-inflammatory cytokine IL-10 was significantly reduced (Fig. 2D) in the H_2S group compared with the control group. These results indicate that an acute H_2S exposure induces a systemic immune response, hypoxia, and liver dysfunction in pig.

3.2. Acute H_2S exposure induced tissue injury and histopathology in lung, trachea and liver of pig

The histological changes of porcine lung, trachea and liver tissues were examined by H.E. staining (Fig. 3). The histological structures of lung, trachea and liver tissues in the Control group (Fig. 3A, B, E, F, I and J) displayed normal morphologies. However, in the H_2S group we observed a considerable inflammatory cell infiltration in the alveolar cells and hyperplasia in the alveolar septums (Fig. 3C and D), which indicated that acute H_2S exposure induced inflammatory lesions in the lung of pig. As shown in Fig. 3G and H, noticeable disruption and desquamation of ciliated epithelial cells within the trachea were observed. There was a massive infiltration of inflammatory cells in the lesions of the trachea after acute H_2S exposure. Vacuolation of hepatocytes was markedly observed in the liver of the H_2S group (Fig. 3K and L), indicating that liver damage was induced by acute H_2S exposure.

3.3. Proteome changes in lung, trachea and liver in response to the acute H_2S exposure

A total of 2770, 3142, and 2629 proteins (Supplemental Table 2) were identified from lung, trachea and liver by quantitative proteomics analysis, respectively. After statistical analysis, 51 (33 increased and 18 decreased), 99 (44 increased and 55 decreased) and 84 (27 increased and 57 decreased) proteins (Supplemental Table 3) with fold change >1.2 and p-value <0.05 were confidently identified as DAPs for lung, trachea and liver between the H_2S group and the Control group.

The volcano plot (Supplemental Fig. S1 A–C) illustrated the proteins changed considerably between H_2S group and Control group in lung, trachea and liver tissues respectably. The heat map results of the hierarchical cluster analysis for the DAPs between the H_2S group and the Control group are shown in Supplemental Fig. S1D–F.

3.4. Bioinformatics analyses of DAPs in lung, trachea and liver

In order to functionally classify the DAPs in response to H_2S treatment, gene ontology (GO) analysis (Supplemental Table 4) was performed with the proteins functional categories including biological processes (BP), cellular components (CC), and molecular functions (MF) for lung, trachea and liver DAPs respectively (Fig. 4A–C). Fig. 4A showed the annotated GO terms of DAPs in lung covering negative regulation of endopeptidase activity, hyaluronan and cholesterol metabolic process, and collagen fibril organization as major subcategories of BP. Extracellular space, extracellular region, spherical high-density lipoprotein particle, heterotrimeric G-protein complex are the key subcategories of CC. Serine-type endopeptidase inhibitor activity, endopeptidase inhibitor activity, hyaluronic acid binding, protein homodimerization activity and serine-type endopeptidase activity are the pivotal MF subcategories. As shown in Fig. 4B, the annotated GO terms of DAPs in trachea contain hyaluronan metabolic process, plasminogen activation, oxidation-reduction process and cilium movement as BP major subcategories. Meanwhile, extracellular space, extracellular region and fibrinogen complex were primary items in CC subcategories; structural molecule activity, serine-type endopeptidase inhibitor activity and signaling receptor binding were predominant hits in MF subcategories. As shown in Fig. 4C, the annotated GO terms of DAPs in liver include translation, oxidation-reduction process and acyl-CoA metabolic process as BP major subcategories; cytoplasm, spliceosomal tri-snRNP complex and actin cytoskeleton as CC subcategories; protein homodimerization activity, RNA binding and structural constituent of ribosome as MF subcategories.

KEGG pathway analysis for the DAPs (Supplemental Table 4) from lung, trachea and liver showed some significantly enriched KEGG pathways in a tissue specific manner as presented in Fig. 4D–F. Specifically, in lung, the most enriched pathways were complement and coagulation cascades, antigen processing and presentation and cell adhesion molecules (CAMs). Similarity in trachea, the most enriched pathways were complement and coagulation cascades, biosynthesis of amino acids and pentose phosphate pathway. The most enriched pathways in liver included metabolic pathways, protein processing in endoplasmic reticulum and primary bile acid biosynthesis.

VENN analysis (Supplemental Table 5) was performed for DAPs, KEGG pathways and GO terms for the three examined porcine organs. The results of VENN analysis showed both the common and unique DAPs and pathways among the lung, trachea and liver of pig after acute exposure to H_2S as presented in Supplemental Fig. S2.

Based on the GO and KEGG results of the DAPs, we focused on more details of key KEGG pathways and GO terms with a significant corrected p value of <0.05 (Table 1), which could potentially be involved in the complex mechanisms of tissue-specific injury induced by acute H_2S exposure.

In addition, the network analysis results for PPI of DAPs were shown in Fig. 5. In the PPI network for lung as depicted in Fig. 5A, 43 of 51 DAPs were detected and 18 of them clustered a network with 26 edges. In the PPI network for trachea as depicted in Fig. 5B, 80 of 99 DAPs were detected and 41 of them constituted a network with 48 edges. In the PPI network for liver as depicted in Fig. 5C, 70 of 84 DAPs were detected and 40 of them constituted a network with 37 edges. We observed functional modules related to 'Complement and coagulation cascades', 'Antigen processing and presentation' and 'Hyaluronan metabolic process' in the PPI network of lung. Also functional modules related to 'Complement and coagulation cascades', 'Oxidation-reduction process and cell proliferation' were found in the PPI network of trachea, and functional modules related to 'Protein synthesis', 'Oxidation-reduction process' and 'Lipid metabolism' were observed in the PPI network of liver. These observations shed some light on the complex response processes in these three organs after acute H_2S exposure in pig.

3.5. Validation of DAPs from proteomics analysis

To validate the DAPs identified and quantified by proteomics analysis, we further performed western blotting analysis as an orthogonal technology to LC-MS-based proteomics using the same aliquots of the proteomic samples for four selected DAPs of biological interest in this study (Fig. 6). BBOX1, HSPA8 and HGD proteins were isolated from liver, and PGD protein was isolated from trachea. In pigs exposed to H_2S, the abundance of BBOX1, HSPA8 and PGD proteins was decreased, while that of HGD was increased compared to the Control group (Fig. 6A and B). The Western blotting results are in a good agreement with the fold changes found in proteomics data (Fig. 6C).

4. Discussion

Acute exposure to H_2S is characterized as a concentration- and time-related toxicity which predominantly affects the nervous, respiratory, digestive and cardiovascular systems (Anantharam et al., 2017; Chen et al., 2019; Schroeter et al., 2006; Yin et al., 2020). There are more than one thousand annual reports related to severe H_2S exposure in the Unites States alone (ATSDR, 2016). However, the clear mechanisms of H_2S-induced multiple organs toxicity have not been elucidated yet, which has delayed the development of suitable countermeasures for treatment after an H_2S intoxication (ATSDR, 2016; Kim et al., 2018; Kim et al., 2020). Existing animal experiments such as those performed with anesthetized mice in an H_2S inhalation exposure model or with rats that were intraperitoneally injected with sodium hydrosulfide (NaHS) do not faithfully reflect the common route of exposure in humans (Jiang et al., 2016; Sonobe et al., 2015).

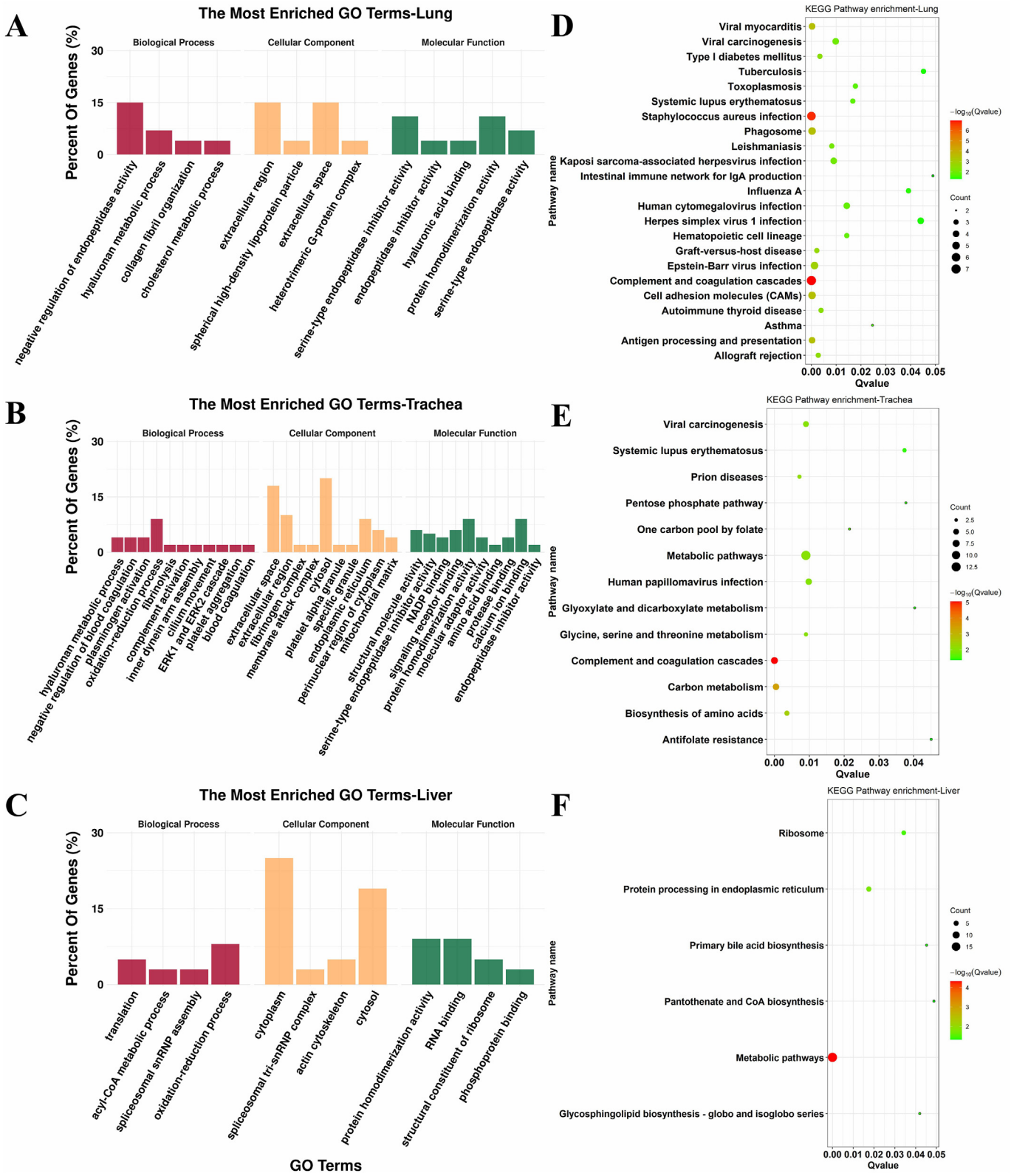

Fig. 4. Gene ontology (GO) annotation and KEGG analyses of DAPs for lung, trachea and liver between H_2S group and Control group. The most enriched GO terms of DAPs in lung (A), trachea (B) and liver (C). The most enriched KEGG pathways of DAPs in lung (D), trachea (E) and liver (F). GO Terms and pathways with corrected p value < 0.05 are shown here.

Moreover, pigs share high similarity to humans in organ structure and genome than any other animal models except primates (Bassols et al., 2014; Reczyńska et al., 2018). Therefore, in this study, we used an inhalation pig model of acute 250 ppm H_2S exposure, which induced multiple organs injuries and allowed us to focus on the lung, trachea and liver for investigation of tissue-specific toxic mechanisms. To the best of our knowledge, this is the first report of applying such a model to mimic an acute H_2S poisoning in human.

Initial investigation of hematological changes including RBC, HGB and HCT levels in the porcine blood suggests a hypoxia condition

Table 1
Key KEGG pathways, GO terms and related proteins were identified in this study.

Accession	Description	Gene Symbol	Fold change (H_2S/Control)	p-Value
Lung				
KEGG:ssc04610 Complement and coagulation cascades				
F1RZN7	Kallikrein B1	KLKB1	1.64	2.59E-02
A0A287BD18	Complement factor H	CFH	1.36	4.49E-02
A0A287AQ20	Complement factor I	CFI	1.26	4.05E-02
F1SB81	Plasminogen	PLG	1.52	1.14E-02
A0A287B9B3	Alpha-2-antiplasmin isoform X2	SERPINF2	1.25	4.55E-02
F1SBS4	Complement C3	C3	1.35	4.63E-02
F1RKY2	Serpin family D member 1	SERPIND1	1.37	4.68E-02
KEGG:ssc04612 Antigen processing and presentation				
A0A088CPQ8	MHC class II antigen	SLA-DRB1	0.41	3.67E-02
Q8MHT8	MHC class I antigen	SLA-3	1.32	1.18E-02
Q04967	Heat shock 70 kDa protein 6	HSPA6	0.76	2.69E-02
A0A160EBY9	MHC class II antigen	SLA-DRA	0.77	3.65E-02
GO:0030212 Hyaluronan metabolic process				
F1SH96	Inter-alpha-trypsin inhibitor heavy chain H1	ITIH1	1.80	3.40E-02
O02668	Inter-alpha-trypsin inhibitor heavy chain H2	ITIH2	1.50	2.13E-02
A0A287BQK2	Inter-alpha-trypsin inhibitor heavy chain H3	ITIH3	1.44	2.99E-02
Trachea				
KEGG:ssc04610 Complement and coagulation cascades				
F1SMJ1	Complement component C7	C7	1.20	2.32E-02
A0A287A6Q0	Vitamin K-dependent protein S	PROS1	1.29	2.91E-02
P14460	Fibrinogen alpha chain (Fragment)	FGA	2.07	2.06E-02
A0SEH3	Complement component C8G	C8G	1.29	3.29E-03
I3LJW2	Fibrinogen gamma chain	FGG	2.14	3.19E-02
Q9GLP2	Vitamin K-dependent protein C	PROC	0.75	4.11E-02
K9J6H8	Alpha-2-macroglobulin	A2M	1.67	1.01E-02
KEGG:ssc01230 Biosynthesis of amino acids				
K7GL74	Ribose-phosphate diphosphokinase	PRPS2	1.33	3.11E-02
A0A287BKR2	Serine hydroxymethyltransferase	SHMT2	1.42	3.05E-02
A0A286ZN35	Serine hydroxymethyltransferase	SHMT1	2.47	1.39E-02
A0A287AJQ2	Phosphoglycerate mutase	PGAM1	0.83	4.97E-02
KEGG:ssc00260 Glycine, serine and threonine metabolism				
A0A287BKR2	Serine hydroxymethyltransferase	SHMT2	1.42	3.05E-02
A0A286ZN35	Serine hydroxymethyltransferase	SHMT1	2.47	1.39E-02
A0A287AJQ2	Phosphoglycerate mutase	PGAM1	0.83	4.97E-02
KEGG:ssc00030 Pentose phosphate pathway				
F1RIF8	6-phosphogluconate dehydrogenase, decarboxylating	PGD	0.76	4.88E-02
K7GL74	Ribose-phosphate diphosphokinase	PRPS2	1.33	3.11E-02
GO:0030212 Hyaluronan metabolic process				
F1SH96	Inter-alpha-trypsin inhibitor heavy chain H1	ITIH1	1.40	1.27E-02
O02668	Inter-alpha-trypsin inhibitor heavy chain H2	ITIH2	1.41	2.07E-02
F1SH92	Inter-alpha-trypsin inhibitor heavy chain H4	ITIH4	1.38	2.71E-02
GO:0055114 Oxidation-reduction process				
A0A287APZ8	Superoxide dismutase	SOD2	0.81	3.14E-02
F1SDB7	Flavin-containing monooxygenase	FMO5	1.72	3.33E-02
K7GR01	Dual oxidase 1	DUOX1	0.72	2.71E-02
F1SNJ5	3-oxo-5-beta-steroid 4-dehydrogenase isoform 1	AKR1D1	2.90	5.66E-03
A0A287AU33	NADPH--cytochrome P450 reductase	POR	1.45	2.13E-02
I3L769	Procollagen-proline 4-dioxygenase	P4HA2	1.31	3.55E-02
K7GKW6	Pirin	PIR	0.68	1.88E-02
GO:0070371 ERK1 and ERK2 cascade				
B2CNZ8	Cathepsin H (Fragment)	CTSH	0.69	2.11E-02
F2Z558	Tyrosine 3-monooxygenase/tryptophan 5-monooxygenase activation protein zeta	YWHAZ	0.81	2.57E-02
GO:0036159 inner dynein arm assembly/GO:0003341 cilium movement				
I3LNF2	Dynein axonemal heavy chain 1	DNAH1	1.64	2.96E-02
A0A287A8I6	Zinc finger MYND domain-containing protein 10 isoform 1	ZMYND10	0.82	1.92E-02
Liver				
KEGG:ssc04141 Protein processing in endoplasmic reticulum				
F1S596	Glucosidase 2 subunit beta	PRKCSH	0.70	2.40E-02
F1RW78	Signal sequence receptor subunit alpha	SSR1	3.02	1.06E-02
I3LRG0	Dolichyl-diphosphooligosaccharide–protein glycosyltransferase subunit 2	RPN2	1.24	3.30E-02
F1S9Q3	Heat shock cognate 71 kDa protein	HSPA8	0.80	3.32E-02
F1SP32	UV excision repair protein RAD23	RAD23B	0.75	1.00E-02
KEGG:ssc00120 Primary bile acid biosynthesis				
F1SGH9	Acyl-coenzyme A oxidase	ACOX2	1.30	8.94E-03
I3LA89	Acyl-CoA thioesterase 8	ACOT8	0.77	1.76E-02
GO:0055114 Oxidation-reduction process				
F1SGL4	Gamma-butyrobetaine hydroxylase 1	BBOX1	0.78	1.11E-02
F1RIX8	Carbonyl reductase 4	CBR4	0.71	4.45E-02
Q28943	Dihydropyrimidine dehydrogenase [NADP(+)]	DPYD	0.83	2.92E-02
I3LLU0	Glycerol-3-phosphate dehydrogenase [NAD(+)]	GPD1L	0.81	4.03E-02
I3LTZ3	Homogentisate 1,2-dioxygenase	HGD	2.45	1.53E-02
A0A287AH74	Corticosteroid 11-beta-dehydrogenase isozyme 1	HSD11B1	1.89	3.61E-02

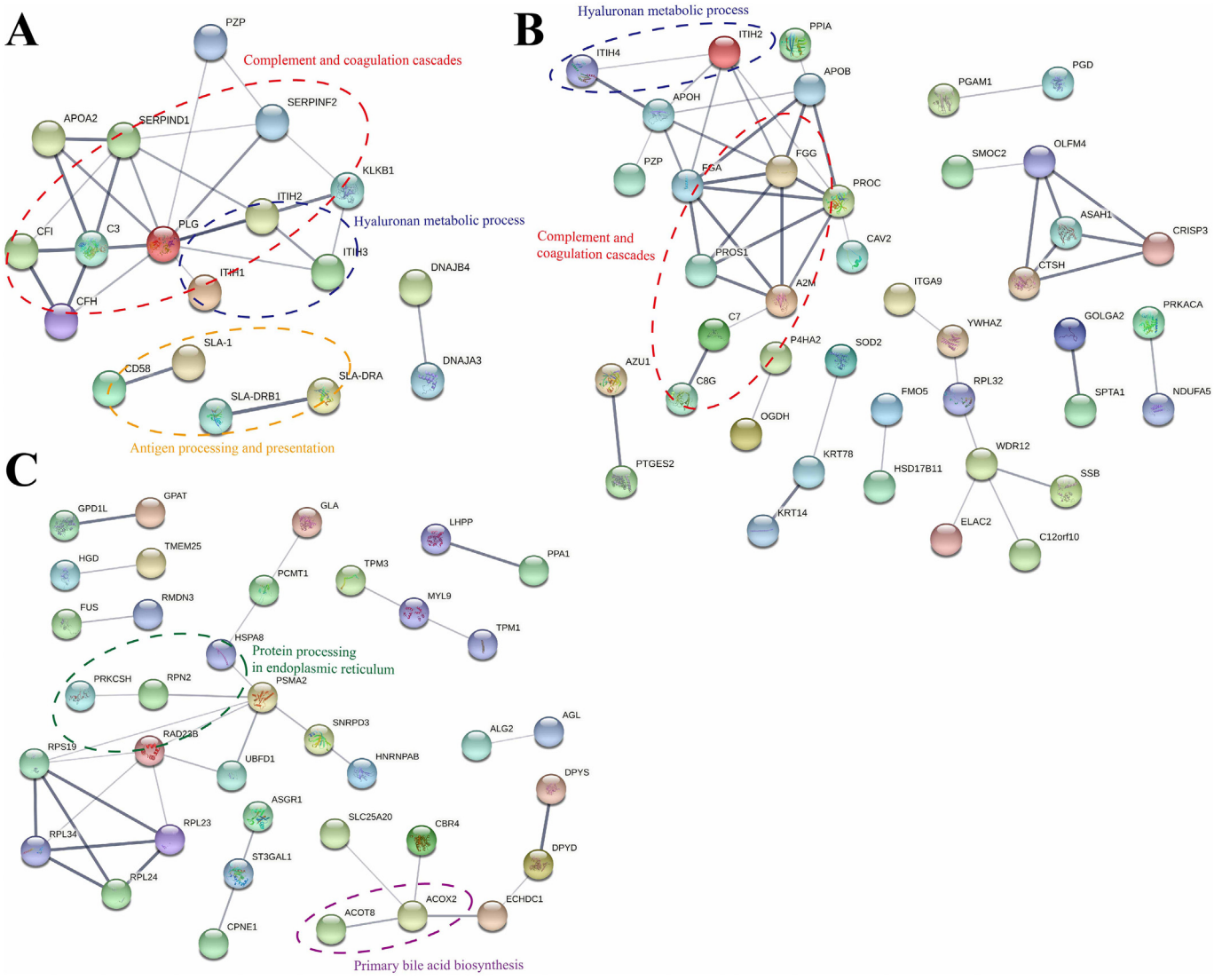

Fig. 5. Protein-protein interaction (PPI) network analysis of DAPs identified in three organs of pig after acute exposure to H_2S. PPI analysis results of DAPs identified in lung (A), trachea (B) and liver (C) of pig after acute exposure to H_2S. Medium-confidence interactions (score ≥ 0.4) were chosen. Line thickness indicates the strength of data support.

induced by acute H_2S exposure in pig (Huerta-Sánchez et al., 2014; Simonson et al., 2010; Yan et al., 2015). That is consistent with what have been reported in an acute H_2S inhalation model in mouse (Kim et al., 2018). Meanwhile, significantly changes in other hematological indexes including WBC, GRA, GRA% and PLT, and serum biochemical indexes including IgA and IgM suggests the occurrence of systemic immune response in pig after an acute H_2S exposure (Anaya-Loyola et al., 2019; Imamoglu et al., 2019; Reddy et al., 2018). More interestingly, we found that pro-inflammatory cytokines (TNF-α, IL-1β and IL-6,) were significantly increased, whereas the level of anti-inflammatory cytokine IL-10 was significantly decreased following acute H_2S exposure in the serum of pigs. These results support the notion that an acute H_2S exposure stimulates a systemic immune response and the occurrence of inflammation in pig (Chi et al., 2018). To fill the mechanistic gap of how acute H_2S exposure induces multiple organs toxicity with a systemic immune response, we sought to probe the proteome profiles of acute H_2S-induced toxicity in lung, trachea and liver using a global proteomic approach. We aim to provide novel insights into the toxicity mechanisms that will ultimately pave the way for the development of antidotes/therapies for the treatment of H_2S intoxication in human.

Many studies have been focusing on exogenous H_2S exposure induced pathological damages in the respiratory tract of human and animals (Song et al., 2021). In a previous study, we reported that H_2S can cause immune suppression, inflammatory response, and cell death in the porcine lung (Liu et al., 2020). Here, in H_2S group of our extended study on acute H_2S exposure, we observed inflammatory cell infiltration and hyperplasia in the alveolar septums in the porcine lung, ciliated epithelial cells disruption and inflammatory cells infiltration in the trachea. Interestingly, the results of the VENN analysis showed that 3 common KEGG pathways (complement and coagulation cascades, systemic lupus erythematosus, and viral carcinogenesis) and 2 common biological processes (hyaluronan metabolic process and negative regulation of endopeptidase activity) of GO analyses were enriched in both lung and trachea (Supplemental Fig. 2). These data suggest a high degree of similarity in response to H_2S exposure between lung and trachea.

One common signaling pathway in lung and trachea, complement and coagulation cascades, plays an important role in host immune defense (Keragala et al., 2018). Seven DAPs in the lung, including KLKB1, CFH, CFI, PLG, SERPINF2, C3 and SERPIND1 were enriched in this pathway. However, seven other DAPs in this pathway, including C7, PROS1, FGA, C8G, FGG, PROC and A2M, were enriched in the trachea. The plasma protein alpha 2-antiplasmin (α2AP), also known as SERPINF2, is an important inhibitor of the serine protease plasmin, which takes place in the dissolution of fibrin clots in blood (Holmes et al., 1987). The alternative pathway of complement activation involves

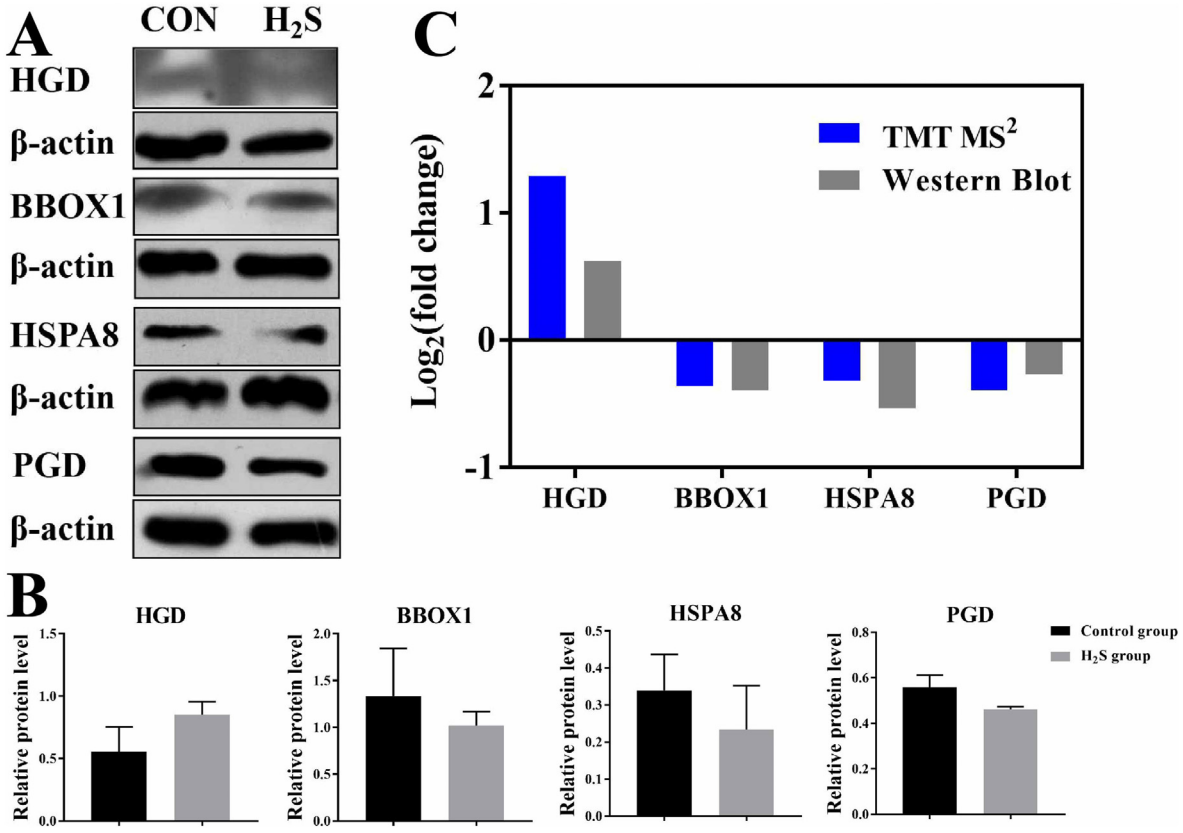

Fig. 6. Validation of proteomics analysis results for four selected DAPs by Western blotting. BBOX1, HSPA8 and HGD proteins were isolated from liver, and PGD protein was isolated from trachea. CON, Control group, $n = 3$; H_2S, H_2S group, $n = 3$. β-actin was used as an internal control for Western blotting.

the spontaneous hydrolysis of C3 and the generation of C3b (Nesargikar et al., 2012). Complement factor H (CFH) serves as a cofactor of Complement factor I (CFI) for regulating the activity of C3b (Alrahmani and Willrich, 2018). The kallikrein B1 (KLKB1), a key molecule in the coagulation pathway, has been reported to inhibit the proteolysis of C5 and regulate the product of active C3 fragments (DiScipio, 1982; Hiemstra et al., 1985; Oikonomopoulou et al., 2012; Thoman et al., 1984). Directly or indirectly, some coagulation proteins affect inflammatory responses and induce lung injury by regulating the level of cytokines or the activation of immune cells (Welty-Wolf et al., 2002). As an important component in immune response, the activation of complement anticipates lung injury in lung disease (Pandya and Wilkes, 2014). In our study, the increase of KLKB1, PLG, and SERPINF2 occurred under the acute H_2S exposure signals that the coagulation cascades were activated in the lung. Furthermore, the significantly higher abundance level of C3, CFH, and CFI suggested that the H_2S exposure activated the alternative pathway of complement activation in the lung. Therefore, acute H_2S exposure may cause the activation of complement and coagulation cascades, which, in turn, induces an inflammatory response in the lung. Similar to this, our previous study found that 20 ppm H_2S exposure for a period of 28 days caused immune response and inflammation in the lung of pig through activating complement system (Liu et al., 2020). The fibrinogen alpha (FGA) and fibrinogen gamma (FGG) are two primary polypeptide chains of fibrinogen (Theodoraki et al., 2010). The Protein C (PROC) is proved to participate in the biological process of coagulation, inflammation, and cell death (Esmon, 2003; Mosnier et al., 2006). The increased abundance of FGA and FGG reflected that the H_2S exposure activated fibrinogen formation in the trachea. Fibrinogen is considered to play a role in inflammation responses by activating proinflammatory pathways, which includes the triggering of NF-κB, and this may result in the production of inflammatory cytokines (Fan and Edgington, 1993; Perez et al., 1999). C7, C8G were also increased in the trachea after the H_2S exposure. C5b-6 can bind C7 and C8G in a sequential manner and forms a terminal complement complex (Nauta et al., 2004). These data suggests that the H_2S exposure may cause inflammation responses by promoting the level of fibrinogen and facilitating the assembly of the complement complex in trachea.

In addition, hyaluronan metabolic processes were found to be increased in both the lung and trachea (Table 1). Hyaluronan is a major component of the extracellular matrix, which plays an important role in regulating inflammation responses (Petrey and de la Motte, 2014). ITIH1, ITIH2, ITIH3 and ITIH4 are important accessories of inter-alpha-trypsin inhibitors (ITIHs), which covalently link to hyaluronan (Hamm et al., 2008). Thus, ITIHs are crucial factors for extracellular matrix stability. ITIH1, ITIH2 and ITIH3 were found in the top 10 list with increased abundance of DAPs in the lung, suggesting that the anti-inflammatory responses during H_2S exposure induced inflammation in the lung. In the trachea, ITIH1, ITIH2 and ITIH4 were increased, suggesting a similar inflammatory response in the trachea as in the lungs.

There are six common DAPs shared between lung and trachea, however some of which not intrinsically belong to these common pathways. Among these DAPs, Paraoxonase 1 (PON1) is related to lipid metabolism (Meneses et al., 2019), and ITIH1 and ITIH2 are associated with the hyaluronan metabolic process (Hamm et al., 2008). Protein S100-A6 (S100A6) is an intracellular protein that regulates cellular proliferation, apoptosis and cellular response to stress factors (Donato et al., 2017). These results help to explain the inflammatory damage occurring in the lung and trachea of pig after 5-h acute H_2S exposure.

Many studies have found that air pollution can affect and modify the antigen presentation process (Becker and Soukup, 2003; Saxon and Diaz-Sanchez, 2005). Here, we observed a unique signaling pathway in the lung, named antigen processing and presentation (Table 1). We found that H_2S exposure increased the abundance of MHC Class I

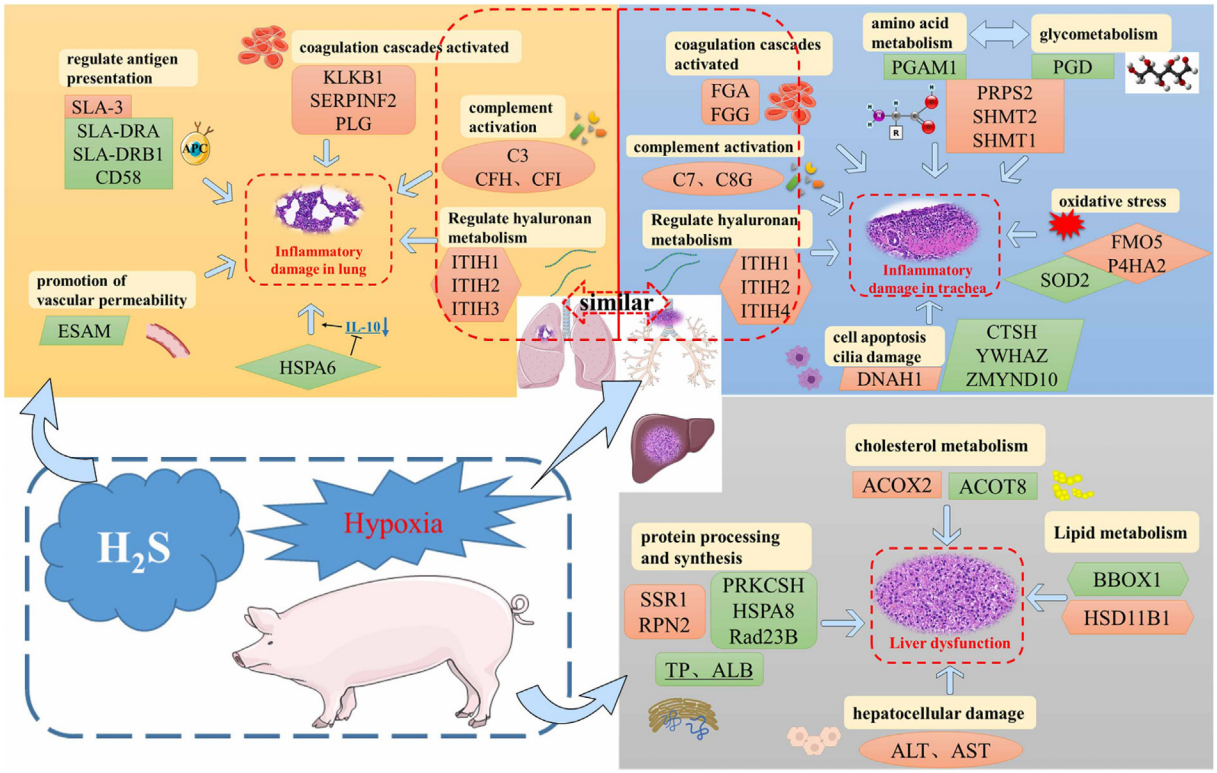

Fig. 7. Overarching scheme of acute H_2S exposure induced multiple organs toxicity in pig. The acute H_2S exposure induced inflammatory injury and dysfunction in lung, trachea and liver via different mechanisms. This figure is a summary of the overall hypothesis of the key pathways and related proteins involved in the complex molecular mechanisms of acute H_2S intoxication in three organs of pig. The red background in the picture signifies increased abundance of proteins, and the green background indicates a decreased abundance of proteins. (For interpretation of the references to colour in this figure legend, the reader is referred to the web version of this article.)

(SLA-3) and decreased the abundance of MHC Class II (SLA-DRA, SLA-DRB1) and HSPA6. Among these proteins, HSPA6 is a member of the HSP70 gene family (Banerjee et al., 2014). HSP70 is reported to activate an anti-inflammatory response by regulating the innate immune response through TLR2 and ERK to stimulate the production of IL-10 (Borges et al., 2012). These results imply that H_2S exposure promotes the presentation of endogenous antigens and restrains the presentation of extracellular antigens (Hansen and Bouvier, 2009). Moreover, the decreased abundance of HSPA6 in the H_2S group corresponds with an inflammation in the lung in the H_2S group. CD58, known as the lymphocyte function-associated antigen 3, is expressed on APCs as a cell adhesion molecule (Clark et al., 2012; York and Rock, 1996). In our study, CD58 was found in the top 10 of decreased abundance proteins, which also suggests that the H_2S exposure affects the antigen presentation in the lung. A similar condition was also found in the previous study, which reported that antigen processing and presentation was regulated in the porcine lung after H_2S exposure (Liu et al., 2020). We also noticed that the H_2S exposure decreased endothelial cell-selective adhesion molecule (ESAM) in the lung. ESAM is a member of the immunoglobulin superfamily, and it is related to endothelial tight junctions (Kimura et al., 2010; Wegmann et al., 2004). Inactivation of ESAM can cause the promotion of vascular permeability in the lung (Duong Cao et al., 2020). The lower ESAM level may be one of the key factors causing inflammatory exudation in the lung.

In addition, some metabolic process-related pathways, such as 'Biosynthesis of amino acids' and 'Glycine, serine and threonine metabolism', 'Pentose phosphate pathway', 'Carbon metabolism' and 'Glyoxylate and dicarboxylate metabolism' were only enriched in the trachea (Table 1), which indicated that the amino acid metabolism and glycometabolism were affected by H_2S exposure, and this occurred specifically in the trachea. Furthermore, the abundance of 7 DAPs (Table 1) belonging to the biological process of oxidation-reduction altered in the trachea due to the H_2S exposure. Superoxide dismutase (SOD2) transforms superoxide produced in the mitochondrial electron transport chain into hydrogen peroxide and diatomic oxygen and wipes out mitochondrial reactive oxygen species, which is significant for protecting cells from cell death (Pias et al., 2003). Flavin-containing monooxygenase (FMO5) is an effective Baeyer–Villiger monooxygenase of the FMO family. Procollagen-proline 4-dioxygenase (P4HA2) belongs to the family of 2-oxoglutarate dependent oxygenases (Rose et al., 2011). The increased abundance of FMO5 and P4HA2, and the decreased SOD2 indicates the H_2S exposure caused oxidative stress in the trachea. Many reports noted that H_2S exposure-induced oxidative stress play an important role in the trachea injury in chicken (Chen et al., 2019; Song et al., 2021). According to the GO analysis, two DAPs from the trachea, CTSH and YWHAZ were enriched in the ERK1 and ERK2 cascade. Increased abundance of Cathepsin H (CTSH) can reduce the cytokine-induced apoptosis (Fløyel et al., 2014). Tyrosine 3-monooxygenase/tryptophan 5-monooxygenase activation protein zeta (YWHAZ) is a major protein for negatively regulating apoptosis and affecting cell survival (Nishimura et al., 2013). Thus, decreased abundance of CTSH and YWHAZ promotes cell apoptosis, which helps to explain the damage of the trachea tissue caused by acute H_2S exposure. Similarly, it was previously shown that H_2S exposure induces apoptosis and necroptosis in broiler trachea (Li et al., 2020). In addition, we also take notice of the fact that there are two DAPs, Dynein axonemal heavy chain 1 (DNAH1) and Zinc finger MYND domain-containing protein 10 (ZMYND10), that are enriched in biological processes of cilium movement and inner dynein arm assembly. As the key component of the outer dynein arm, DNAH1 plays an important role in maintaining ciliary function (Milla, 2016). ZMYND10 is also known for its function in maintaining normal cilia motility (Moore et al., 2013). Thus, the different expression of these two proteins suggests that the H_2S exposure can affect function and motility of the airway cilia. In the histological study regarding the trachea, we also observed an apparent mucosal injury and cilia desquamating. All these results indicate that the H_2S exposure may cause inflammation and cilia injuries in airway

mucosa via activating the complement and coagulation cascades, inducing oxidative stress and cell apoptosis.

There are no shared DAPs and pathways in all three organs while fewer DAPs and pathways shared between lung/trachea and liver, which supports the notion that the exposure of H_2S affects liver via different mechanisms over lung/trachea. For the liver, 5 DAPs were enriched in the pathway of protein processing in the endoplasmic reticulum (Table 1). Signal sequence receptor subunit alpha (SSR1) is one of the signal sequence receptors, and is associated with protein translocation across the endoplasmic reticulum (ER) membrane(Rapoport, 1991). Dolichyl-diphosphooligosaccharide–protein glycosyltransferase (RPN2) is one of the subunits of the oligosaccharyltransferase (OST) complex. OST plays a part in improving the kinetics and thermodynamics of the folding of proteins (Schwarz and Blower, 2016). Protein kinase C substrate 80 K-H (PRKCSH) normally locates in the ER lumen, and PRKCSH is known as the noncatalytic β subunit of glucosidase II (GII) (Shin et al., 2019). Heat shock cognate 71 kDa protein (HSPA8) is an important member of the HSP70 family, and protein folding is also a major cellular function of HSPA8 (Stricher et al., 2013). UV excision repair protein RAD23 (Rad23B) belongs to Rad23 that interacts with the proteasome and escorts Png1p to the proteasome. In this way, Rad23 helps to efficiently deglycosylate the substrate before degradation (Suzuki et al., 2001). The increased SSR1 and decreased PRN2, PRKCSH, HSPA8, and RAD23B suggest that acute H_2S exposure could affect protein processing and synthesis in the endoplasmic reticulum in the liver. We also observed a significantly decline in TP and ALB level and an increasement in serum ALT and AST levels after H_2S exposure. These results indicate that an acute H_2S exposure may cause a hepatocellular damage leading to liver dysfunction (Chen et al., 2009; Heibatollah et al., 2008). H_2S exposure can also exacerbate LPS-induced hepatocyte autophagy in chicken (Guo et al., 2021).

There are two DAPs, acyl-coenzyme A oxidase (ACOX2) and acyl-CoA thioesterase 8 (ACOT8), that were enriched in the pathway of primary bile acid biosynthesis. The bile acid synthesis is important for the catabolism of cholesterol to bile acids. ACOX2 is a rate limiting enzyme associated to the bile acid biosynthetic process (Bjørklund et al., 2015; Ferdinandusse et al., 2018). ACOT8 is involved in the regulation of fatty acid oxidation (Hunt et al., 2012). These data suggested the H_2S exposure affects cholesterol metabolism in the liver via the regulation of the primary bile acid biosynthesis. Moreover, we also found the same biological process of GO analysis in the liver as that in the trachea, the oxidation-reduction process, whereas the belonged proteins were totally different (Table 1). Gamma-butyrobetaine hydroxylase 1 (BBOX1) participates in the carnitine biosynthesis pathway (Paul et al., 1992). Carnitine is important for mitochondrial beta oxidation of fatty acid (Rashidi-Nezhad et al., 2014). Corticosteroid 11-beta-dehydrogenase isozyme 1 (HSD11B1) is a member of the family of short-chain dehydrogenases, which plays an important role in balancing the lipid metabolism (Honma et al., 2012; Oppermann et al., 2003). These data indicates that the H_2S exposure can cause lipometabolic disorder in liver. Similarly, another harmful gas, ammonia, regulates lipid metabolism in the porcine skeletal muscle (Tang et al., 2020).

In conclusion, the acute H_2S exposure affects 3 organs via different mechanisms. An overall scheme of key proteins and their tissue-specific pathways we hypothesize to be involved in the pathogenesis of acute H_2S induced multiple organs toxicity, is summarized in Fig. 7. The toxic mechanisms of H_2S exposure in the lung and trachea are more similar to one another. The H_2S exposure causes inflammatory damages in the lung through the activation of complement and coagulation cascades, promoting antigen-presentation and regulating the hyaluronan metabolic process. In the trachea, the H_2S exposure activated complement and coagulation cascades, caused oxidative stress and cell apoptosis, and regulated the hyaluronan metabolic process. In this way, the H_2S exposure causes inflammatory injury and cilia desquamating. In the liver, the H_2S exposure induces liver dysfunctions via the regulation of protein synthesis and lipid metabolism. Collectively, these findings shed new light on toxic molecular mechanisms that could potentially be targeted for therapeutic intervention for acute H_2S intoxication.

Supplementary data to this article can be found online at https://doi.org/10.1016/j.scitotenv.2021.150365.

CRediT authorship contribution statement

Zhen Liu: Conceptualization, Methodology, Investigation, Writing – original draft. **Liang Chen:** Conceptualization, Resources, Investigation, Writing – review & editing. **Xin Gao:** Formal analysis, Visualization, Writing – original draft. **Ruixia Zou:** Visualization, Investigation, Writing – review & editing. **Qingshi Meng:** Investigation, Formal analysis. **Qin Fu:** Writing – review & editing. **Yanjiao Xie:** Investigation. **Qixiang Miao:** Investigation. **Lei Chen:** Investigation. **Xiangfang Tang:** Conceptualization, Funding acquisition, Supervision, Writing – review & editing. **Sheng Zhang:** Supervision, Writing – review & editing. **Hongfu Zhang:** Conceptualization, Funding acquisition, Supervision, Resources. **Martine Schroyen:** Supervision, Writing – review & editing.

Declaration of competing interest

The authors declare that they have no known competing financial interests or personal relationships that could have appeared to influence the work reported in this paper.

Acknowledgments

This work was supported by the National Key Research and Development Program of China (No. 2016YFD0500501). We are grateful for partial financial support from China Scholarship Council to Zhen Liu in this study (No. 202003250080).

References

Alrahmani, L., Willrich, M.A.V., 2018. The complement alternative pathway and pre-eclampsia. Curr. Hypertens. Rep. 20, 40.

Anantharam, P., Whitley, E.M., Mahama, B., Kim, D.-S., Imerman, P.M., Shao, D., Langley, M.R., Kanthasamy, A., Rumbeiha, W.K., 2017. Characterizing a mouse model for evaluation of countermeasures against hydrogen sulfide–induced neurotoxicity and neurological sequelae. Ann. N. Y. Acad. Sci. 1400, 46.

Anaya-Loyola, M.A., Enciso-Moreno, J.A., López-Ramos, J.E., García-Marín, G., Álvarez, M.Y.O., Vega-García, A.M., Mosqueda, J., García-Gutiérrez, D.G., Keller, D., Pérez-Ramírez, I.F., 2019. Bacillus coagulans GBI-30, 6068 decreases upper respiratory and gastrointestinal tract symptoms in healthy Mexican scholar-aged children by modulating immune-related proteins. Food Res. Int. 125, 108567.

ATSDR, 2016. Toxicological Profile for Hydrogen Sulfide and Carbonyl Sulfide. US Department of Health and Human Services Public Health Service, Agency for Toxic Substances and Disease Registry, p. 298.

Ausma, T., De Kok, L.J., 2019. Atmospheric H2S: impact on plant functioning. Front. Plant Sci. 10, 743.

Banerjee, D., Upadhyay, R.C., Chaudhary, U.B., Kumar, R., Singh, S., Ashutosh, G.J.M., Polley, S., Mukherjee, A., Das, T.K., De, S., 2014. Seasonal variation in expression pattern of genes under HSP70. Cell Stress Chaperon 19, 401–408.

Bassols, A., Costa, C., Eckersall, P.D., Osada, J., Sabrià, J., Tibau, J., 2014. The pig as an animal model for human pathologies: a proteomics perspective. Proteom. Clin. Appl. 8, 715–731.

Becker, S., Soukup, J., 2003. Coarse(PM(2.5-10)), fine(PM(2.5)), and ultrafine air pollution particles induce/increase immune costimulatory receptors on human blood-derived monocytes but not on alveolar macrophages. J. Toxicol. Environ. Health A 66, 847–859.

Bjørklund, S.S., Kristensen, V.N., Seiler, M., Kumar, S., Alnæs, G.I.G., Ming, Y., Kerrigan, J., Naume, B., Sachidanandam, R., Bhanot, G., et al., 2015. Expression of an estrogen-regulated variant transcript of the peroxisomal branched chain fatty acid oxidase ACOX2 in breast carcinomas. BMC Cancer 15, 524.

Borges, T., Wieten, L., van Herwijnen, M., Broere, F., Van Der Zee, R., Bonorino, C., Van Eden, W., 2012. The anti-inflammatory mechanisms of Hsp70. Front. Immunol. 3, 95.

Burnett, W.W., King, E.G., Grace, M., Hall, W.F., 1977. Hydrogen sulfide poisoning: review of 5 years' experience. Can. Med. Assoc. J. 117, 1277–1280.

Chen, J., Xie, P., Li, L., Xu, J., 2009. First identification of the hepatotoxic microcystins in the serum of a chronically exposed human population together with indication of hepatocellular damage. Toxicol. Sci. 108, 81–89.

Chen, M., Li, X., Shi, Q., Zhang, Z., Xu, S., 2019. Hydrogen sulfide exposure triggers chicken trachea inflammatory injury through oxidative stress-mediated FOS/IL8 signaling. J. Hazard. Mater. 368, 243–254.
Chi, Q., Chi, X., Hu, X., Wang, S., Zhang, H., Li, S., 2018. The effects of atmospheric hydrogen sulfide on peripheral blood lymphocytes of chickens: perspectives on inflammation, oxidative stress and energy metabolism. Environ. Res. 167, 1–6.
Chi, Q., Hu, X., Liu, Z., Han, Y., Tao, D., Xu, S., Li, S., 2021. H2S exposure induces cell death in the broiler thymus via the ROS-initiated JNK/MST1/FOXO1 pathway. Ecotoxicol. Environ. Saf. 222, 112488.
Clark, H., Banks, R., Jones, L., Hornick, T., Higgins, P., Burant, C., Canaday, D., 2012. Characterization of MHC-II antigen presentation by B cells and monocytes from older individuals. Clin. Immunol. 144, 172–177.
DiScipio, R.G., 1982. The activation of the alternative pathway C3 convertase by human plasma kallikrein. Immunology 45, 587–595.
Donato, R., Sorci, G., Giambanco, I., 2017. S100A6 protein: functional roles. Cell. Mol. Life Sci. 74, 2749–2760.
Duong Cao, N., Nottebaum Astrid, F., Butz, S., Volkery, S., Zeuschner, D., Stehling, M., Vestweber, D., 2020. Interference with ESAM (endothelial cell-selective adhesion molecule) plus vascular endothelial-cadherin causes immediate lethality and lung-specific blood coagulation. Arterioscler. Thromb. Vasc. Biol. 40, 378–393.
Esmon, C.T., 2003. The protein C pathway. Chest 124, 26S–32S.
Fan, S.T., Edgington, T.S., 1993. Integrin regulation of leukocyte inflammatory functions. CD11b/CD18 enhancement of the tumor necrosis factor-alpha responses of monocytes. J. Immunol. 150, 2972–2980.
Ferdinandusse, S., Denis, S., van Roermund, C.W.T., Preece, M.A., Koster, J., Ebberink, M.S., Waterham, H.R., Wanders, R.J.A., 2018. A novel case of ACOX2 deficiency leads to recognition of a third human peroxisomal acyl-CoA oxidase. BBA-Mol. Basis Dis. 1864, 952–958.
Fløyel, T., Brorsson, C., Nielsen, L.B., Miani, M., Bang-Berthelsen, C.H., Friedrichsen, M., Overgaard, A.J., Berchtold, L.A., Wiberg, A., Poulsen, P., 2014. CTSH regulates β-cell function and disease progression in newly diagnosed type 1 diabetes patients. Proc. Natl. Acad. Sci. U. S. A. 111, 10305–10310.
Guidotti, T.L., 2010. Hydrogen sulfide: advances in understanding human toxicity. Int. J. Toxicol. 29, 569–581.
Guidotti, T.L., 2015. Hydrogen sulfide intoxication. Handb. Clin. Neurol. Elsevier, pp. 111–133.
Guo, J.-M., Xing, H.-J., Cai, J.-Z., Zhang, H.-F., Xu, S.-W., 2021. H2S exposure-induced oxidative stress promotes LPS-mediated hepatocyte autophagy through the PI3K/AKT/TOR pathway. Ecotoxicol. Environ. Saf. 209, 111801.
Hamm, A., Veeck, J., Bektas, N., Wild, P.J., Hartmann, A., Heindrichs, U., Kristiansen, G., Werbowetski-Ogilvie, T., Del Maestro, R., Knuechel, R., Dahl, E., 2008. Frequent expression loss of inter-alpha-trypsin inhibitor heavy chain (ITIH) genes in multiple human solid tumors: a systematic expression analysis. BMC Cancer 8, 25.
Hansen, T.H., Bouvier, M., 2009. MHC class I antigen presentation: learning from viral evasion strategies. Nat. Rev. Immunol. 9, 503–513.
Heibatollah, S., Reza, N.M., Izadpanah, G., Sohailla, S., 2008. Hepatoprotective effect of Cichorium intybus on CCl4-induced liver damage in rats. Afr. J. Biochem. Res. 2, 141–144.
Hendry-Hofer, T.B., Ng, P.C., McGrath, A.M., Mukai, D., Brenner, M., Mahon, S., Maddry, J.K., Boss, G.R., Bebarta, V.S., 2020. Intramuscular aminotetrazole cobinamide as a treatment for inhaled hydrogen sulfide poisoning in a large swine model. Ann. N. Y. Acad. Sci. 1479, 159–167.
Hiemstra, P.S., Daha, M.R., Bouma, B.N., 1985. Activation of factor B of the complement system by kallikrein and its light chain. Thromb. Res. 38, 491–503.
Holmes, W.E., Nelles, L., Lijnen, H.R., Collen, D., 1987. Primary structure of human alpha 2-antiplasmin, a serine protease inhibitor (serpin). J. Biol. Chem. 262, 1659–1664.
Honma, T., Shinohara, N., Ito, J., Kijima, R., Sugawara, S., Arai, T., Tsuduki, T., Ikeda, I., 2012. High-fat diet intake accelerates aging, increases expression of Hsd11b1, and promotes lipid accumulation in liver of SAMP10 mouse. Biogerontology 13, 93–103.
Huerta-Sánchez, E., Jin, X., Bianba, Z., Peter, B.M., Vinckenbosch, N., Liang, Y., Yi, X., He, M., Somel, M., Ni, P., 2014. Altitude adaptation in Tibetans caused by introgression of Denisovan-like DNA. Nature 512, 194–197.
Hughes, M.N., Centelles, M.N., Moore, K.P., 2009. Making and working with hydrogen sulfide: the chemistry and generation of hydrogen sulfide in vitro and its measurement in vivo: a review. Free Radic. Biol. Med. 47, 1346–1353.
Hunt, M.C., Siponen, M.I., Alexson, S.E.H., 2012. The emerging role of acyl-CoA thioesterases and acyltransferases in regulating peroxisomal lipid metabolism. BBA-Mol. Basis Dis. 1822, 1397–1410.
Imamoglu, G.I., Eren, T., Baylan, B., Karacın, C., 2019. May high levels of systemic immune-inflammation index and hematologic inflammation markers suggest a further stage in testicular tumours? Urol. Int. 103, 303–310.
Jiang, J., Chan, A., Ali, S., Saha, A., Haushalter, K.J., Lam, W.-L.M., Glasheen, M., Parker, J., Brenner, M., Mahon, S.B., 2016. Hydrogen sulfide—mechanisms of toxicity and development of an antidote. Sci. Rep. 6, 1–10.
Keragala, C.B., Draxler, D.F., McQuilten, Z.K., Medcalf, R.L., 2018. Haemostasis and innate immunity–a complementary relationship: a review of the intricate relationship between coagulation and complement pathways. Br. J. Haematol. 180, 782–798.
Kim, D.-S., Anantharam, P., Hoffmann, A., Meade, M.L., Grobe, N., Gearhart, J.M., Whitley, E.M., Mahama, B., Rumbeiha, W.K., 2018. Broad spectrum proteomics analysis of the inferior colliculus following acute hydrogen sulfide exposure. Toxicol. Appl. Pharmacol. 355, 28–42.
Kim, D.-S., Anantharam, P., Padhi, P., Thedens, D.R., Li, G., Gilbreath, E., Rumbeiha, W.K., 2020. Transcriptomic profile analysis of brain inferior colliculus following acute hydrogen sulfide exposure. Toxicology 430, 152345.
Kimura, R., Ishida, T., Kuriyama, M., Hirata, K., Hayashi, Y., 2010. Interaction of endothelial cell-selective adhesion molecule and MAGI-1 promotes mature cell-cell adhesion via activation of RhoA. Genes Cells 15, 385–396.
Lewis, R.J., Copley, G.B., 2015. Chronic low-level hydrogen sulfide exposure and potential effects on human health: a review of the epidemiological evidence. Crit. Rev. Toxicol. 45, 93–123.
Li, L., Bhatia, M., Zhu, Y.Z., Zhu, Y.C., Ramnath, R.D., Wang, Z.J., Anuar, F.B.M., Whiteman, M., Salto-Tellez, M., Moore, P.K., 2005. Hydrogen sulfide is a novel mediator of lipopolysaccharide-induced inflammation in the mouse. FASEB J. 19, 1196–1198.
Li, X., Chen, M., Shi, Q., Zhang, H., Xu, S., 2020. Hydrogen sulfide exposure induces apoptosis and necroptosis through lncRNA3037/miR-15a/BCL2-A20 signaling in broiler trachea. Sci. Total Environ. 699, 134296.
Liu, Z., Fu, Q., Tang, S., Xie, Y., Meng, Q., Tang, X., Zhang, S., Zhang, H., Schroyen, M., 2020. Proteomics analysis of lung reveals inflammation and cell death induced by atmospheric H2S exposure in pig. Environ. Res. 191, 110204.
Malone Rubright, S.L., Pearce, L.L., Peterson, J., 2017. Environmental toxicology of hydrogen sulfide. Nitric Oxide-Biol. Chem. 71, 1–13.
Meneses, M.J., Silvestre, R., Sousa-Lima, I., Macedo, M.P., 2019. Paraoxonase-1 as a regulator of glucose and lipid homeostasis: impact on the onset and progression of metabolic disorders. Int. J. Mol. Sci. 20, 4049.
Milla, C.E., 2016. The evolving spectrum of ciliopathies and respiratory disease. Curr. Opin. Pediatr. 28, 339–347.
Moore, D.J., Onoufriadis, A., Shoemark, A., Simpson, M.A., de Castro, S.C., zur Lage, P.I., Bartoloni, L., Gallone, G., Petridi, S., Woollard, W.J., et al., 2013. Mutations in ZMYND10, a gene essential for proper axonemal assembly of inner and outer dynein arms in humans and flies, cause primary ciliary dyskinesia. Am. J. Hum. Genet. 93, 346–356.
Morii, D., Miyagatani, Y., Nakamae, N., Murao, M., Taniyama, K., 2010. Japanese experience of hydrogen sulfide: the suicide craze in 2008. J. Occup. Med. Toxicol. 5, 1–3.
Mosnier, L.O., Zlokovic, B.V., Griffin, J.H., 2006. The cytoprotective protein C pathway. Blood 109, 3161–3172.
Nauta, A.J., Roos, A., Daha, M.R., 2004. A regulatory role for complement in innate immunity and autoimmunity. Int. Arch. Allergy Immunol. 134, 310–323.
Nesargikar, P.N., Spiller, B., Chavez, R., 2012. The complement system: history, pathways, cascade and inhibitors. Eur. J. Microbiol. Immunol. 2, 103–111.
Ng, P.C., Hendry-Hofer, T.B., Witeof, A.E., Brenner, M., Mahon, S.B., Boss, G.R., Haouzi, P., Bebarta, V.S., 2019. Hydrogen sulfide toxicity: mechanism of action, clinical presentation, and countermeasure development. J. Med. Toxicol. 1–8.
Nishimura, Y., Komatsu, S., Ichikawa, D., Nagata, H., Hirajima, S., Takeshita, H., Kawaguchi, T., Arita, T., Konishi, H., Kashimoto, K., et al., 2013. Overexpression of YWHAZ relates to tumor cell proliferation and malignant outcome of gastric carcinoma. Br. J. Cancer 108, 1324–1331.
Oikonomopoulou, K., Ricklin, D., Ward, P.A., Lambris, J.D., 2012. Interactions between coagulation and complement–their role in inflammation. Semin. Immunopathol. 34, 151–165.
Oppermann, U., Filling, C., Hult, M., Shafqat, N., Wu, X., Lindh, M., Shafqat, J., Nordling, E., Kallberg, Y., Persson, B., Jörnvall, H., 2003. Short-chain dehydrogenases/reductases (SDR): the 2002 update. Chem. Biol. Interact. 143–144, 247–253.
Pandya, P.H., Wilkes, D.S., 2014. Complement system in lung disease. Am. J. Respir. Cell Mol. Biol. 51, 467–473.
Paul, H.S., Sekas, G., Adibi, S.A., 1992. Carnitine biosynthesis in hepatic peroxisomes. Eur. J. Biochem. 203, 599–605.
Perez, R.L., Ritzenthaler, J.D., Roman, J., 1999. Transcriptional regulation of the interleukin-1beta promoter via fibrinogen engagement of the CD18 integrin receptor. Am. J. Respir. Cell Mol. Biol. 20, 1059–1066.
Petrey, A., de la Motte, C., 2014. Hyaluronan, a crucial regulator of inflammation. Front. Immunol. 5, 101.
Pias, E.K., Ekshyyan, O.Y., Rhoads, C.A., Fuseler, J., Harrison, L., Aw, T.Y., 2003. Differential effects of superoxide dismutase isoform expression on hydroperoxide-induced apoptosis in PC-12 cells. J. Biol. Chem. 278, 13294–13301.
Rapoport, T.A., 1991. Protein transport across the endoplasmic reticulum membrane: facts, models, mysteries. FASEB J. 5, 2792–2798.
Rashidi-Nezhad, A., Talebi, S., Saebnouri, H., Akrami, S.M., Reymond, A., 2014. The effect of homozygous deletion of the BBOX1 and fibin genes on carnitine level and acyl carnitine profile. BMC Med. Genet. 15, 75.
Reczyńska, K., Tharkar, P., Kim, S.Y., Wang, Y., Pamuła, E., Chan, H.-K., Chrzanowski, W., 2018. Animal models of smoke inhalation injury and related acute and chronic lung diseases. Adv. Drug Deliv. Rev. 123, 107–134.
Reddy, K.E., Song, J., Lee, H.-J., Kim, M., Kim, D.-W., Jung, H.J., Kim, B., Lee, Y., Yu, D., Kim, D.-W., 2018. Effects of high levels of deoxynivalenol and zearalenone on growth performance, and hematological and immunological parameters in pigs. Toxins (Basel) 10, 114.
Reedy, S.J.D., Schwartz, M.D., Morgan, B.W., 2011. Suicide fads: frequency and characteristics of hydrogen sulfide suicides in the United States. West. J. Emerg. Med. 12, 300.
Reiffenstein, R., Hulbert, W.C., Roth, S.H., 1992. Toxicology of hydrogen sulfide. Annu. Rev. Pharmacol. Toxicol. 32, 109–134.
Rose, N.R., McDonough, M.A., King, O.N.F., Kawamura, A., Schofield, C.J., 2011. Inhibition of 2-oxoglutarate dependent oxygenases. Chem. Soc. Rev. 40, 4364–4397.
Roura, E., Koopmans, S.-J., Lallès, J.-P., Le Huerou-Luron, I., de Jager, N., Schuurman, T., Val-Laillet, D., 2016. Critical review evaluating the pig as a model for human nutritional physiology. Nutr. Res. Rev. 29, 60–90.
Saiyed, H., 2006. Hydrogen sulfide: human health aspects, concise international chemical assessment document No. 53. Indian J. Med. Res. 123, 96.
Saxon, A., Diaz-Sanchez, D., 2005. Air pollution and allergy: you are what you breathe. Nat. Immunol. 6, 223–226.

Schroeter, J.D., Kimbell, J.S., Andersen, M.E., Dorman, D.C., 2006. Use of a pharmacokinetic-driven computational fluid dynamics model to predict nasal extraction of hydrogen sulfide in rats and humans. Toxicol. Sci. 94, 359–367.
Schwarz, D.S., Blower, M.D., 2016. The endoplasmic reticulum: structure, function and response to cellular signaling. Cell. Mol. Life Sci. 73, 79–94.
Shin, G.-C., Moon, S.U., Kang, H.S., Choi, H.-S., Han, H.D., Kim, K.-H., 2019. PRKCSH contributes to tumorigenesis by selective boosting of IRE1 signaling pathway. Nat. Commun. 10, 3185.
Simonson, T.S., Yang, Y., Huff, C.D., Yun, H., Qin, G., Witherspoon, D.J., Bai, Z., Lorenzo, F.R., Xing, J., Jorde, L.B., 2010. Genetic evidence for high-altitude adaptation in Tibet. Science 329, 72–75.
Snyder, J.W., Safir, E.F., Summerville, G.P., Middleberg, R.A., 1995. Occupational fatality and persistent neurological sequelae after mass exposure to hydrogen sulfide. Am. J. Emerg. Med. 13, 199–203.
Song, N., Li, X., Cui, Y., Zhang, T., Xu, S., Li, S., 2021. Hydrogen sulfide exposure induces pyroptosis in the trachea of broilers via the regulatory effect of circRNA-17828/miR-6631-5p/DUSP6 crosstalk on ROS production. J. Hazard. Mater. 418, 126172.
Sonobe, T., Chenuel, B., Cooper, T.K., Haouzi, P., 2015. Immediate and long-term outcome of acute H2S intoxication induced coma in unanesthetized rats: effects of methylene blue. PLoS One 10, e0131340.
Stricher, F., Macri, C., Ruff, M., Muller, S., 2013. HSPA8/HSC70 chaperone protein: structure, function, and chemical targeting. Autophagy 9, 1937–1954.
Suzuki, T., Park, H., Kwofie, M.A., Lennarz, W.J., 2001. Rad23 provides a link between the Png1 deglycosylating enzyme and the 26 S proteasome in Yeast*. J. Biol. Chem. 276, 21601–21607.
Tang, S., Xie, J., Wu, W., Yi, B., Liu, L., Zhang, H., 2020. High ammonia exposure regulates lipid metabolism in the pig skeletal muscle via mTOR pathway. Sci. Total Environ. 740, 139917.
Theodoraki, E.V., Nikopensius, T., Suhorutšenko, J., Peppes, V., Fili, P., Kolovou, G., Papamikos, V., Richter, D., Zakopoulos, N., Krjutškov, K., et al., 2010. Fibrinogen beta variants confer protection against coronary artery disease in a greek case-control study. BMC Med. Genet. 11, 28.
Thoman, M.L., Meuth, J.L., Morgan, E.L., Weigle, W.O., Hugli, T.E., 1984. C3d-K, a kallikrein cleavage fragment of iC3b is a potent inhibitor of cellular proliferation. J. Immunol. 133, 2629–2633.
Wegmann, F., Ebnet, K., Du Pasquier, L., Vestweber, D., Butz, S., 2004. Endothelial adhesion molecule ESAM binds directly to the multidomain adaptor MAGI-1 and recruits it to cell contacts. Exp. Cell Res. 300, 121–133.
Welty-Wolf, K.E., Carraway, M.S., Ortel, T.L., Piantadosi, C.A., 2002. Coagulation and inflammation in acute lung injury. Thromb. Haemost. 88, 17–25.
Yan, Y., Shi, Y., Wang, C., Guo, P., Wang, J., Zhang, C.-Y., Zhang, C., 2015. Influence of a high-altitude hypoxic environment on human plasma microRNA profiles. Sci. Rep. 5, 1–10.
Yin, K., Cui, Y., Qu, Y., Zhang, J., Zhang, H., Lin, H., 2020. Hydrogen sulfide upregulates miR-16-5p targeting PiK3R1 and RAF1 to inhibit neutrophil extracellular trap formation in chickens. Ecotoxicol. Environ. Saf. 194, 110412.
York, I.A., Rock, K.L., 1996. Antigen processing and presentation by the class I major histocompatibility complex. Annu. Rev. Immunol. 14, 369–396.